Joint Pathology Center
Veterinary Pathology Services

WEDNESDAY SLIDE CONFERENCE 2025-2026

Conference #15 — 14 January 2026

CASE I:

Signalment:
29 week old, intact female, C57BL/6NCrl mouse (*Mus musculus*)

History:
This animal was utilized in a study of chronic kidney disease and was euthanized at a pre-defined study endpoint.

Gross Pathology:
The body weight was 14 g and the mouse had decreased fat stores. Bilaterally the kidneys were diffusely pale-tan and shrunken with a pitted appearance and miliary white depressed foci.

Laboratory Results:
Serum chemistry demonstrated elevated BUN (94 mg/dL; ref 5-28), creatinine (0.54 mg/dL; ref 0.20-0.50), globulin (2.9 g/dL; ref 1.7-2.2), and phosphorous (15.4 mg/dL; ref 7.3-14.5).

Complete blood count demonstrated a microcytic, hypochromic, regenerative anemia (HCT 33.2%, ref 37.2-62.0; MCV 36.1 fL, ref 42.6-56.0; MCH 11.3 pg, ref 13-16.8; RET 603.8 K/uL, ref 294-444).

Automated leukocyte differential demonstrated leukopenia (3.26 K/uL, ref 3.9-13.96) characterized by a lymphopenia (0.82 K/uL, ref 2.88-10.92).

Urine specific gravity was low (1.015, ref 1.050-1.093).

Microscopic Description:
Kidney. The surface of the renal cortex is undulating with an irregular, scalloped appearance. Multifocally, renal tubules are dilated and have an attenuated epithelium. Dilated tubules are variably filled with an amorphous, pale basophilic material or abundant degenerate neutrophils, and less commonly contain brown to pale basophilic, spiculated, radiating birefringent crystalline material (2,8-dihydroxyadenine crystals) or dark basophilic coarsely granular material Occasionally, crystal-filled tubules are surrounded by neutrophils, macrophages, and multinucleated giant cells. Often, Bowman's spaces are mild to moderately dilated. Throughout the renal parenchyma, between tubules are streams of fibroblasts and collagen.

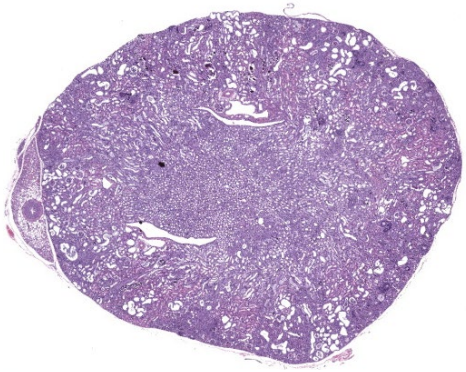

Figure 1-1. Kidney, mouse: At sub-gross magnification, groups of ectatic tubules are present in the cortex along with abundant mineral. The capsule has an undulant profile. (HE, 10X)

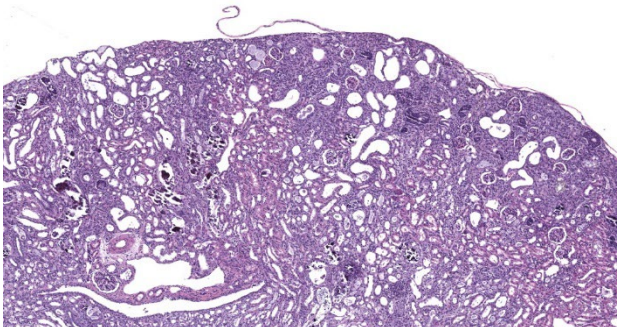

Figure 1-2. Kidney, mouse: Within the cortex, regional groups of tubules demonstrate ectasia with epithelial attenuation, loss of cytoplasmic eosinophilic eosinophilia, and mineralization. (HE, 94X)

Contributor's Morphologic Diagnoses:

Liver: Microvesicular hepatopathy, moderate, acute, diffuse, with mild centrilobular hepatocellular necrosis.

Contributor's Comment:

This mouse was administered 0.2% adenine in the diet for six weeks as part of a study on CKD. The animal was part of the control group and received no experimental manipulations except for adenine administration. The adenine diet model is a commonly utilized, well-established model of chronic kidney disease (CKD) in mice and rats.[9] This diet induces a tubulointerstitial nephritis secondary to the metabolism of adenine in the kidneys. Adenine is metabolized by the enzyme xanthine dehydrogenase into 2,8-dihydroxyadenine (DHA), which precipitates in renal tubules, resulting in crystal formation.[16] Injury of the tubules leads to tubulointerstitial inflammation which progresses over time to interstitial fibrosis.[15] The model mirrors some of the clinicopathologic findings observed in human and animal CKD, including azotemia, hyperphosphatemia, elevated parathyroid hormone (PTH), and anemia.[4,13,16] This model is well-established and reproducible in rodents, and while it has also been described in rabbits it is not well characterized in this species.[5]

Naturally occurring chronic renal disease in mammals typically results in non-regenerative anemia due to decreased production of erythropoietin, increased hepcidin, suppression of erythropoiesis, and decreased red blood cell lifespan.[11] Studies of the adenine diet model of chronic kidney disease in rodents have demonstrated variation in the nature of the resulting anemia. Some studies employing the adenine diet model to study anemia of CKD have demonstrated no difference in absolute reticulocyte count between anemic and non-anemic animals, consistent with a non-regenerative response that is expected in a model of CKD-associated anemia.[2, 17] However, others have demonstrated anemia with an increase in absolute reticulocyte count in rodents consuming a high-adenine diet.[1] In the course of this study, we have observed an apparent regenerative response characterized by increased reticulocytes in adenine-treated mice. The mechanism for reticulocytosis in the face of overt renal insufficiency is not yet understood.

Rodents consuming a high-adenine diet begin to demonstrate evidence of renal injury, including reduction in creatinine clearance and intraluminal crystals, starting on day 3 after diet initiation.[10] DHA crystals are brown, spiculated spheres which are birefringent in polarized light microscopy. Kidney lesions progresses as the diet is maintained, with tubular damage as the primary lesion. Crystals are primarily localized to proximal tubules and ascending limbs of the loops of Henle.[10] Glomeruli are not directly injured by DHA nephropathy; however, dilation of the Bowman's space is reported as a histologic finding of the adenine diet model.[9] Direct tubular injury is accompanied by inflammation characterized primarily by macrophages which accumulate around injured tubules.[10,15] Over time,

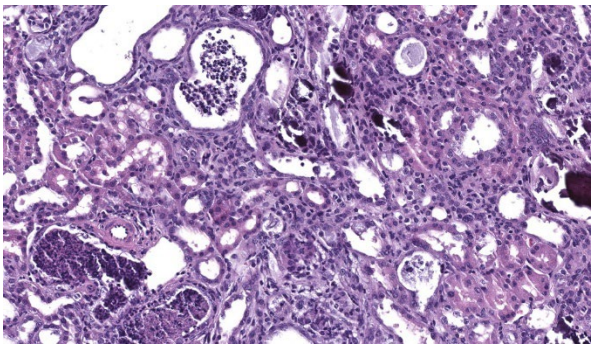

Figure 1-3. Kidney, mouse: Higher magnification of tubular changes with ectasia, collapse, proteinosis, mineralization, infiltration of tubular lumens with necrotic neutrophils, and expansion of the interstitium with macrophages and mild fibrosis. (HE, 381)

tubular injury and inflammation progresses to interstitial fibrosis.

In humans, an inherited defect in purine metabolism leads to the accumulation of DHA and subsequent DHA nephrolithiasis. This autosomal recessive disorder results from a mutation of the gene encoding the enzyme adenine phosphoribosyltransferase (APRT), which normally catalyzes the formation of 5'-adenosine monophosphate (AMP) from adenine.[3] Without this enzyme, adenine is instead metabolized to DHA which, as in the mouse model, precipitates within renal tubules and causes crystalline nephropathy. The mechanisms of the adenine diet in rodents closely recapitulate this human disease, making the adenine diet model a suitable preclinical model APRT deficiency.[10] While the currently reported prevalence of APRT deficiency in human populations is quite low, this may represent an under-reporting of disease frequency.[3] Biochemical stone analysis fails to differentiate DHA from uric acid, so stereomicroscopic analysis of urinary stones and infrared spectroscopy are preferable.[3]

DHA nephrolithiasis, likely caused by a similar genetic mutation, has been reported rarely in dogs.[6, 8] There is a breed predisposition for primitive-type breeds such as malamutes and Native American Indian dogs. The genetic mutation identified in affected dogs is a missense mutation of the *APRT* gene.[6] Clinically, affected animals have been documented to develop uroliths throughout the upper and lower urinary tract, which in some cases progress to obstructive renal failure. Treatment, as in humans, is administration of xanthine dehydrogenase inhibitors such as allopurinol.

Multiple drugs and toxins are capable of causing renal intratubular crystallization and subsequent damage. Ethylene glycol and melamine/cyanuric acid toxicosis are two examples of crystal nephropathy of veterinary importance. In contrast to DHA precipitation in the adenine diet model, ethylene glycol (EG) and melamine/cyanuric acid ingestion result in calcium oxalate monohydrate crystals or melamine-containing crystals, respectively. In EG toxicosis, EG metabolism results in the production of several end products, including oxalic acid. Oxalic acid binds to calcium within renal tubules and forms calcium oxalate crystals, which are directly cytotoxic and results in renal tubular epithelial cell death.[12] The mechanism of melamine renal toxicity is less clearly elucidated, but co-administration of melamine and cyanuric acid appears necessary to induce crystal formation.[14] Presence of melamine/cyanuric acid crystals within renal tubules is associated with tubular epithelial necrosis.[7]

Contributing Institution:
Laboratory of Comparative Pathology, Memorial Sloan Kettering Cancer Center, The Rockefeller University, Weill Cornell Medicine. https://www.mskcc.org/research/ski/core-facilities/comparative-medicine-pathology-0

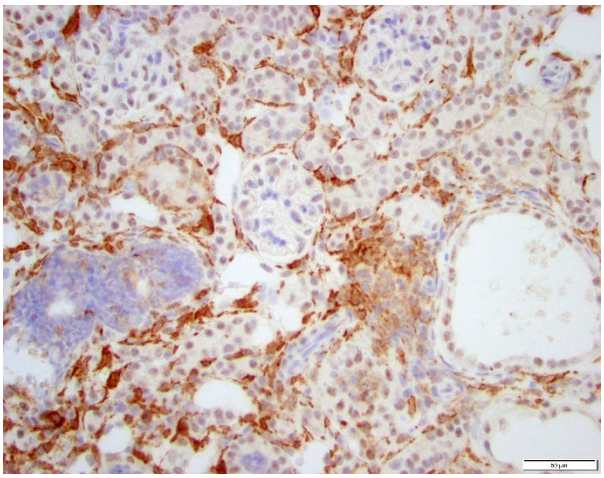

Figure 1-4. Kidney, mouse: There are moderate numbers of IBA-1 immunopositive macrophages withi the interstitium. (anti-IBA-1, 400X)) (Photo courtesy of: Laboratory of Comparative Pathology, Memorial Sloan Kettering Cancer Center, The Rockefeller University, Weill Cornell Medicine. https://www.mskcc.org/research/ski/core-facilities/comparative-medicine-pathology-0)

JPC Diagnoses:
Kidney, cortex: Tubular degeneration, necrosis, and regeneration, chronic, diffuse, marked, with intratubular and interstitial crystals, granular and hyaline casts, mineralization, and interstitial fibrosis.

JPC Comment:
Conference 15 was moderated by the globally renowned Dr. Cory Brayton, a top expert in mouse pathology from Johns Hopkins School of Medicine. This first case is one that has never been seen before in the WSC, and the contributor provided an outstanding write-up to accompany it.

Conference discussion covered multiple topics, some of which are covered in the provided write-up. Dr. Brayton spoke on numerous important features in the evaluation of a case such as this. These included knowing the history of the affected animal, understanding common background lesions in particular mice strains, and where the discerning pathologist should look for mineral in the kidneys (within tubules, in tubular basement membranes, and within vascular tunics). Additionally, emphasis was placed on ensuring one takes the time to evaluate the presence or absence of tubular degeneration, regeneration, and/or atrophy (all of which were present in this case as tubular damage is the primary lesion of adenine nephritis), and the histologic appearance of crystals. There was some speculation amongst participants on the presence of tubular regeneration in this slide, which is typically characterized by hypercellular, more basophilic tubules with a high N:C ratio in their epithelial cells. Ultimately, the presence of regenerative tubules was agreed upon, although it took the more experienced eyes in the room to point them out to less experienced participants. The Non-Neoplastic Lesion Atlas and Mouse INHAND guide both have excellent examples of tubular regeneration for those that may be unfamiliar.[6,16] There was discussion on how to discern atrophy of brown fat after one participant questioned if the adipose tissue in the slide was atrophic or just brown fat (it was brown fat), which is challenging, but best assessed around the salivary gland in mice. Atrophic brown fat has the appearance of being its own unidentifiable organ due to the degree of consolidation; don't be fooled!

There was significant discussion on the complete blood count (CBC) of this case, which demonstrated a microcytic, hypochromic, regenerative anemia. This struck conference participants as odd since most chronic kidney disease (CKD) patients have a normochromic, non-regenerative anemia due to the lack of erythropoietin production from the damaged kidneys. Additionally, the reticulocyte count was reportedly elevated, which should have

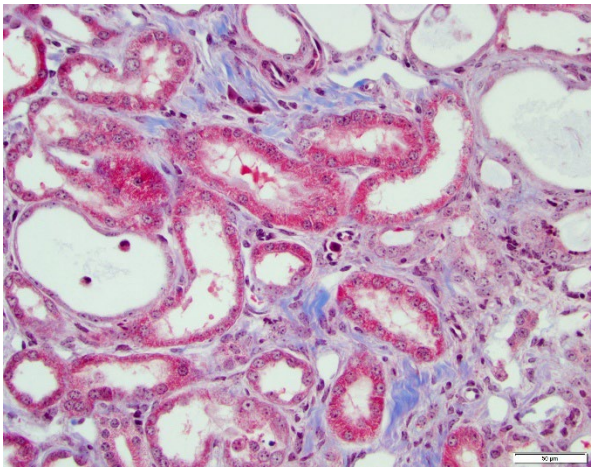

Figure 1-5. Kidney, mouse: A Masson's trichrome stain highlights the mild interstitial fibrosis. (Masson's, 400X) (Photo courtesy of: Laboratory of Comparative Pathology, Memorial Sloan Kettering Cancer Center, The Rockefeller University, Weill Cornell Medicine. https://www.mskcc.org/research/ski/core-facilities/comparative-medicine-pathology-0).

resulted in macrocytosis rather than microcytosis. The blood chemistry profile of this animal also revealed an elevated BUN, mildly elevated creatinine, mildly elevated globulin, and mild hyperphosphatemia. While these findings indicate an azotemia was present, the elevated globulin and phosphorus levels may suggest that this animal was dehydrated and had a pre-renal azotemia rather than renal azotemia. Urine specific gravity (USG) and total protein (TP) measurements would have helped tease this out further, but conference participants acknowledge that there are limitations in some cases. Additionally, most laboratories have their own reference ranges for different strains of mice that often differ from those used in other labs, so conference participants assumed that this contributor's lab knows their reference ranges in this particular mouse strain and deferred to their data in drawing these conclusions. It certainly made for excellent discussion!

While the history of an adenine diet in this mouse made for a straightforward diagnosis, other possible causes of brown crystals in kidneys include melamine cyanuric acid, bilirubin, calcium carbonate, and ammonium biurate, to name the most pertinent. Additional causes of proximal convoluted tubular (PCT) damage in other species that win honorable mentions from conference discussion include aminoglycosides (foals and humans), oxalates (ruminants), monensin (horses and poultry), and ethylene glycol (dogs, cats, and humans).

Lastly, wrapping up discussion was a quick mention by Dr. Brayton on the potential for Mouse Kidney Parvovirus (MKPV) to confound CKD studies in mice. In a recent study, it was found that MKPV-infected mice on an adenine diet for CKD study had more interstitial nephritis at one month and two months of diet consumption compared to those that did not have MKPV.[15] They also had less interstitial fibrosis at 2 months comparatively.[15] This virus, which makes for some stunning histologic images, by the way (please see the cover of the new Barthold book), can complicate grading and evaluation of CKD-associated lesions in mice that are infected during the study period and, as such, lesions should be interpreted with caution and contexts.

References:

1. Akchurin O, Patino E, Dalal V, et al. Interleukin-6 contributes to the development of anemia in juvenile CKD. *Kidney International Reports*. 2019;4:470-483.
2. Akchurin O, Sureshbabu A, Doty SB, et al. Lack of hepcidin ameliorates anemia and improves growth in an adenine-induced mouse model of chronic kidney disease. *Am J Physiol Renal Physiol*. 2016;311(5):F877-F889.

3. Bollee G, Harambat J, Bensman A, Knebelmann B, Daudon M, Ceballos-Picot I. Adenine Phosphoribosyltransferase Deficiency. *Clin J Am Soc Nephrol*. 2012;7:1521-1527.
4. deFrutos S, Luengo A, Garcia-Jerez A, et al. Chronic kidney disease induced by an adenine rich diet upregulates integrin linked kinase (ILK) and its depletion prevents the disease progression. *BBA Molecular Basis of Disease.* 2019;1865:1284-1297.
5. Florens N, Lemoine S, Pelletier CC, Rabeyrin M, Juillard L, Soulage CO. Adenine Rich Diet Is Not a Surrogate of 5/6 Nephrectomy in Rabbits. *Nephron*. 2017;135:307-314.
6. Frazier KS, Seely JC, Hard GC, et al. Proliferative and nonproliferative lesions of the rat and mouse urinary system. *Toxicol Pathol*. 2012;40(4 Suppl):14S-86S.
7. Furrow E, Pfeifer RJ, Osborne CA, Lulich JP. An APRT mutation is strongly associated with and likely causative for 2,8-dihydroxyadenine urolithiasis in dogs. *Mol Genet Metab.* 2014;111(3):399-403.
8. Hau AK, Kwan TH, Li PK. Melamine Toxicity and the Kidney. *J Am Soc Nephrol.* 2009;20:145-250.
9. Houston DM, Moore AE, Mendonca SZ, Taylor JA: 2,8-Dihydroxyadenine uroliths in a dog. *J Am Vet Med Assoc*. 2012;241:1348–1352.
10. Jia T, Olauson H, Lindberg K, et al. A novel model of adenine-induced tubulointerstitial nephropathy in mice. *BMC Nephrology.* 2013;14:116.
11. Klinkhammer BM, Djudjaj S, Kunter U, et al. Cellular and Molecular Mechanisms of Kidney Injury in 2,8-Dihydroxyadenine Nephropathy. *J Am Soc Nephrol.* 2020;31:799-816.
12. Lippi I, Perondi F, Lubas G, et al. Erythrogram patterns in dogs with chronic kidney disease. *Vet Sci*. 2021;8(7):123.
13. McMartin K. Are calcium oxalate crystals involved in the mechanism of acute renal failure in ethylene glycol poisoning? *Clinical Toxicology*. 2009;47(9):859-869.
14. Rahman A, Yamazaki D, Sufiun A, et al. A novel approach to adenine-induced chronic kidney disease associated anemia in rodents. *PLoS ONE*. 2018;13(2): e0192531.
15. Ritter AC, Arbona RRJ, Livingston RS, Monette S, Lipman NS. Effects of Mouse Kidney Parvovirus on Pharmacokinetics of Chemotherapeutics and the Adenine Model of Chronic Kidney Disease. *Comp Med*. 2023;73(2):153-172.
16. Sands JM, Verlander JW. Anatomy and physiology of the kidneys. In: Toxicology of the Kidney, 3rd ed (Tarloff JB, Lash LH, eds). CRC Press, Boca Raton, FL. 2005;3-56.
17. Son JY, Kang YJ, Kim KS, et al. Evaluation of Renal Toxicity by Combination Exposure to Melamine and Cyanuric Acid in Male Sprague-Dawley Rats. *Toxicol*. Res. 2014;30(2):99-107.
18. Tamura M, Aizawa R, Hori M, Ozaki H. Progressive renal dysfunction and macrophage infiltration in interstitial fibrosis in an adenine-induced tubulointerstitial nephritis mouse model. *Histochem Cell Biol*. 2009;131:483-490.

19. Tani T, Orimo H, Shimizu A, Tsuruoka S. Development of a novel chronic kidney disease mouse model to evaluate the progression of hyperphosphatemia and associated mineral bone disease. *Scientific Reports*. 2017;7:2233.
20. Thibodeau JF, Simard JC, Holterman CE, et al. PBI-4050 via GPR40 activation improves adenine-induced kidney injury in mice. *Clin Sci (Lond)*. 2019;133(14):1587-1602.

CASE II:

Signalment:
21-year-old, intact male, rhesus macaque, (*Macaca mulatta*)

History:
This Indian-origin rhesus macaque has a history of oral and dental disease. Approximately four months prior to necropsy, heavy dental calculus, gingivitis, and loose teeth necessitated cleaning and extraction of multiple teeth. The extraction sites did not heal despite several therapies. Radiographs revealed a retained tooth fragment and an oronasal fistula. The dental fragment was removed and this surgical site also failed to heal. Incisional biopsies of the palatine mucosa and buccal mucosa were collected and microscopic evaluation revealed an ameloblastoma. Euthanasia was elected.

Gross Pathology:
Well-muscled, aged, intact male rhesus monkey in excellent nutritional condition (body weight 11.8, body condition score 3/5). Expanding the buccal mucosa and gingiva adjacent to the dental extraction sites and invading the hard palate is a pale, white, glistening neoplasm that measures up to 3.6 cm in greatest dimension (tissue not submitted). The gastric mucosa is diffusely and moderately thickened

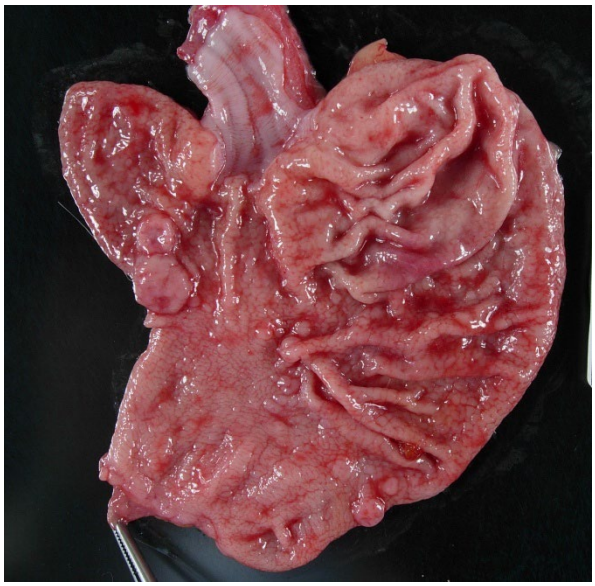

Figure 2-1. Stomach, rhesus macaque: Numerous round, fleshy, dark pink, sessile tumors protrude from the gastric mucosa into the lumen and measure up to 1 cm in diameter (Photo courtesy of: Oregon National Primate Research Center, https://www.ohsu.edu/onprc).

and exhibits a cobblestone pattern. Round, fleshy, dark pink, sessile tumors protrude from the gastric mucosa into the lumen and measure up to 1 cm in diameter. There are multiple outpouchings of the intestinal mucosa (diverticulosis). The free margins of the left atrioventricular valve are minimally thickened and nodular (endocardiosis). The aortic intima is multifocally thickened with raised white to yellow irregular plaques (atherosclerosis). Few cysts measuring up to 0.2 cm in diameter are present in both renal cortices.

Laboratory Results:
N/A.

Microscopic Description:
Focally elevating the attenuated, intact superficial epithelium and expanding the gastric mucosa and submucosa and displacing gastric

Figure 2-2. Stomach, rhesus macaque: Two full-thickness sections of stomach are submitted for examination. (HE, 9X)

glands are multiple, coalescing, partially encapsulated multilobulated neoplasms composed of nests and packets of neoplastic cells supported by a fine fibrovascular stroma.

)Some rosette formation with luminal blood is present and in other areas, there is pseudoglandular formation with entrapment of glands and foveolar epithelium. Neoplastic cells are round to polygonal with variably indistinct cell borders and amphophilic to pale eosinophilic, lightly granular cytoplasm. Nuclei are round to oval with usually one distinct nucleolus and finely dispersed to coarsely stippled chromatin. Occasionally, neoplastic cells contain up to three nuclei. There is moderate to marked anisocytosis and anisokaryosis and less than one mitotic figure/HPF. Submucosal vascular invasion is present. There is proprial edema overlying mucosal nodules. Moderate numbers of plasma cells and lymphocytes, fewer eosinophils, and occasional macrophages, neutrophils, and Mott cells are present within the lamina propria and multifocally traverse the muscularis mucosa and extend to the submucosa. Multifocally, there is foveolar hyperplasia and dysplasia and expansion of the mucosa-associated lymphoid tissue. The submucosa is variably edematous and lymphatic vessels are ectatic.

Contributor's Morphologic Diagnoses:

1. Stomach: Neuroendocrine tumor (carcinoid), multiple, mucosa and submucosa with vascular invasion.

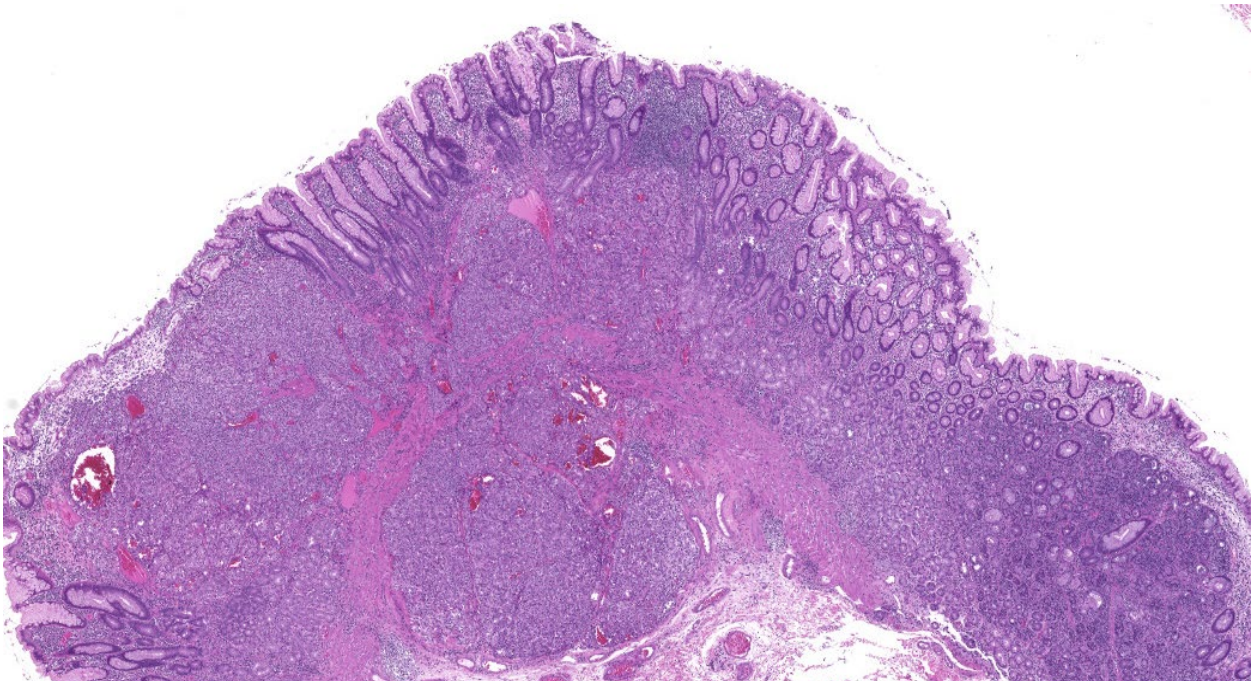

Figure 2-3. Stomach, rhesus macaque: There is a neoplasm infiltrating the gastric mucosa and underlying submucosa. (HE, 44X)

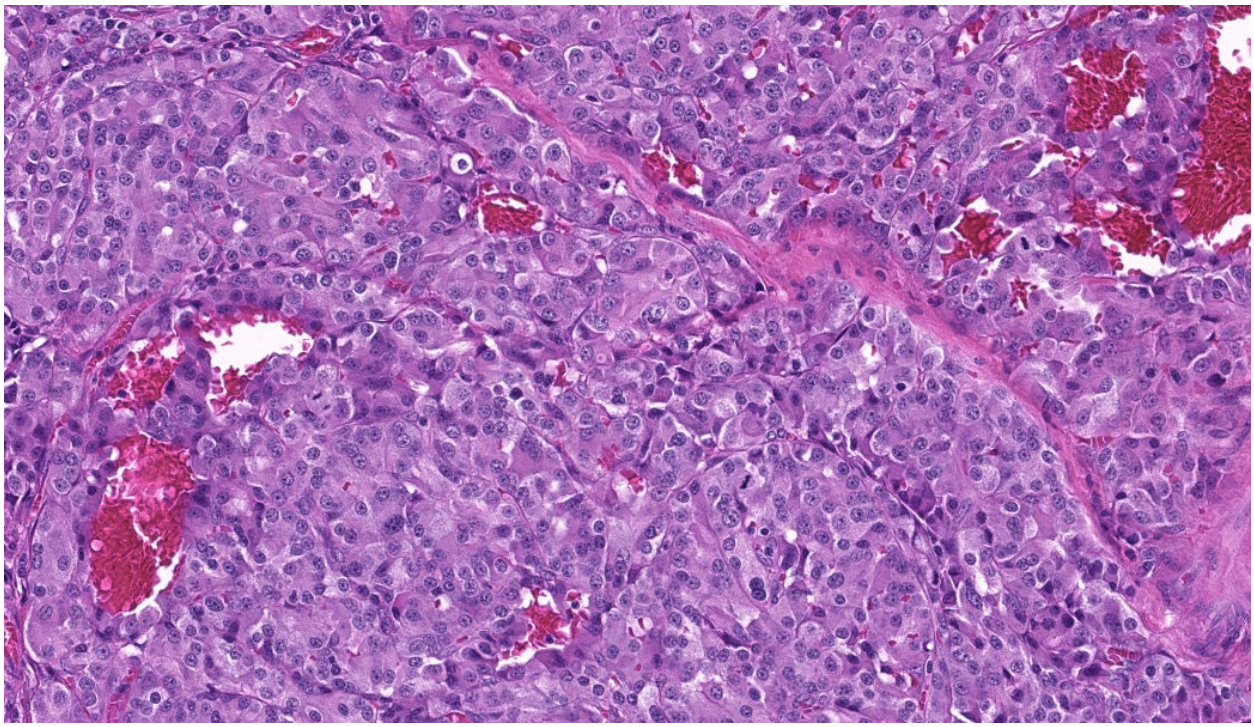

Figure 2-4. Stomach, rhesus macaque: Neoplastic cells are arranged in nests and packets. (HE, 306X)

2. Stomach: Gastritis, plasmacytic, lymphocytic, few eosinophils and occasional macrophages, neutrophils, and Mott cells, diffuse, moderate, with multifocal, mild foveolar hyperplasia and dysplasia.

Contributor's Comment:

This macaque had multiple malignant gastric carcinoids. Vascular invasion was evident in the vasculature of the submucosa; however, regional or distant metastases were not identified on microscopic examination of remaining tissues. A Churukian-Schenk histochemical stain highlighted argyrophilic granules within neoplastic cells, and neoplastic cells were also immunoreactive for chromogranin A, a neuroendocrine marker (fig. 3). The histologic features, immunohistochemical and special histochemical staining of these neoplasms were consistent with the diagnosis of carcinoids.

Gastric carcinoid tumors arise from the neuroendocrine cells of the mucosa and are rare in this large nonhuman primate colony. A retrospective review of pathology records spanning the last six decades at the center revealed only one other case of gastric carcinoid in an adult female rhesus macaque. A single, malignant carcinoid that exhibited lymphatic invasion was diagnosed. During a recent virtual conference, multiple neuroendocrine gastric neoplasms were reported in an aged rhesus macaque. (Ruivo, P. 2023, April 25. Gastric Neuroendocrine Tumor, NHPRC Virtual Slide Conference, California National Primate Research Center, UC Davis School of Veterinary Medicine.) A review of the literature revealed rare reports of carcinoid tumors involving sites other than the stomach in nonhuman primates and included hepatic carcinoid tumors in a baboon (Papio sp.) and a Japanese macaque (Macaca fuscata), the lung of a rhesus macaque (Macaca mulatta), and the duodenum of a cynomolgus macaque (Macaca fascicularis).[2,4,5,7]

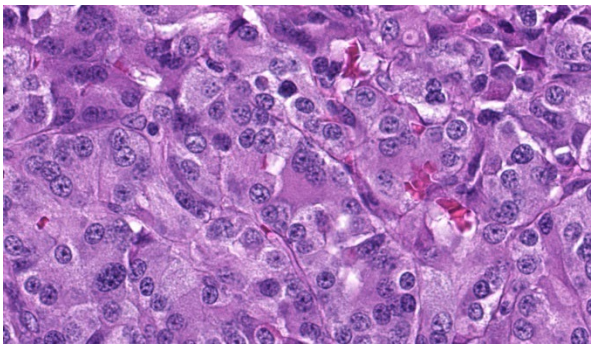

Figure 2-5. Stomach, rhesus macaque: High magnification of neoplastic cells, which have abundant granular cytoplasm, minimal atypia, and a low mitotic rate. (HE, 306X)

In humans, gastric carcinoids may be solitary or multiple and are placed in three categories. Type 1 presents with multiple, slow growing tumors. Local and distant metastases are rare. The pathogenesis is thought to involve chronic atrophic gastritis where there is parietal cell loss resulting in achlorhydria which causes excessive release of gastrin from G cells. Hypergastrinemia stimulates tumor formation and growth. Type 2 carcinoids are associated with gastrinomas; hypergastrinemia occurs because of a primary increase in gastric acid production. These carcinoids are associated with Zollinger-Ellison syndrome and generally occur in patients with MEN type I. Tumors are small, multiple, slow growing, and metastasize more often when compared to type 1. Type 3 carcinoids are usually solitary, rapidly growing, and exhibit frequent metastases to regional lymph nodes and the liver. They are not associated with chronic atrophic gastritis, gastrinomas, or MEN 1, and may be composed of multiple kinds of endocrine cells. Blood gastrin levels are normal. Atypical carcinoid syndrome characterized by flushing may be seen.[13] The classification scheme for human carcinoids could not be applied in this case. There were multiple tumors in this macaque. The functionality of the tumors is unknown. Clinical signs such as nausea, vomiting, diarrhea, and sustained weight loss consistent with Zollinger-Ellison syndrome were not reported. Chronic, atrophic gastritis was not evident on microscopic examination.

Spontaneous gastric neuroendocrine tumors are rare in domestic veterinary species.[1,12] Other species reported with spontaneous gastric neuroendocrine tumors include a ferret (Mustela putorius furo), an aged Sprague-Dawley Rat, and 7/135 striped field mice (Apodemus agrarius).[3,8,9] At least two species are an exception to the rarity of gastric carcinoids noted here. A retrospective study of neoplasia in the alimentary tract of bearded dragons (Pogona spp) reported that of 26 gastric neoplasms, 16 were neuroendocrine carcinomas. Metastases were observed in 14 of these cases most often to the liver and kidney reflecting an aggressive biologic behavior.[6] In another study involving bearded dragons, 5 of 5 tumors demonstrated immunolabeling for somatostatin.[10] Spontaneous gastric carcinoids were diagnosed on necropsies of 600 African rodents, Praomys (Mastomys) natalensis housed in a closed colony. Two-thirds of the aged males and one-third of the aged females were affected and exhibited regional and distant metastases.[11]

Contributing Institution:
Pathology Services Unit
Division of Animal Resources and Research Support
Oregon National Primate Research Center
505 NW 185th Avenue
Beaverton, OR 97006
https://www.ohsu.edu/onprc

JPC Diagnoses:
1. Stomach: Neuroendocrine tumor (carcinoid).
2. Stomach: Gastritis, lymphoplasmacytic, chronic, diffuse, moderate.

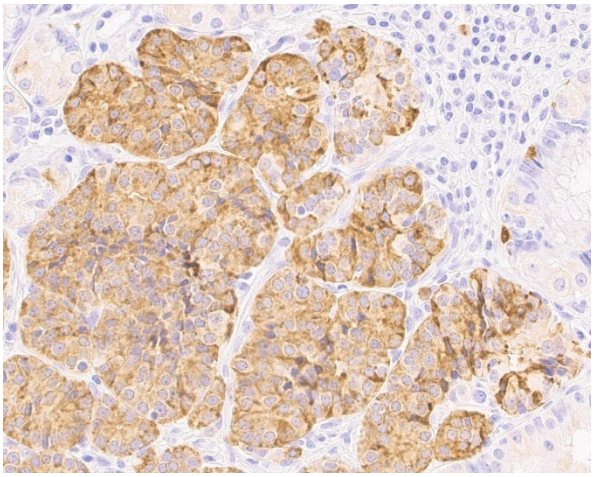

Figure 2-6. Stomach, rhesus macaque: Neoplastic cells demonstrate strong diffuse cytoplasmic immunopositivity for chromogranin A. (anti-chromogranin A, 400X) (Photo courtesy of: Oregon National Primate Research Center, https://www.ohsu.edu/onprc)

JPC Comment:

Another fantastic write-up! This case made for highly educational discussion on a classic entity. Many thanks to the contributor for providing this case, along with chromogranin A IHC images that supported the diagnosis. Chromogranin A is a great IHC to use for these types of cases, as it immunoreacts with dense granules in neuroendocrine cells. Other great IHC options for neuroendocrine neoplasms include synaptophysin or insulinoma-associated protein-1 (INSM-1).

Most participants were initially split on this diagnosis based on the H&E alone, with some confidently diagnosing a carcinoid and others wondering about an adenocarcinoma due to the formation of what appeared to be acini. The presence of nests, packets, pseudoglandular formation, and rosettes in the neoplasm's pattern should clue the pathologist into the possibility that this is a neuroendocrine neoplasm rather than an epithelial one. Participants engaged in spirited debate on the presence of vascular invasion in this digital-only case. Most participants were not sold on it and interpreted the nucleated cells within blood vessels as either histiocytes or other nucleated circulating cells. Ultimately, IHC would have been necessary to confirm this. As such, vascular invasion was left out of the JPC's morphologic diagnosis. Participants did agree that the gastritis should receive its own morphologic diagnosis, as most did not think it was simply a result of the neoplasm due to the prevalence of gastritis, enteritis, and colitis seen in captive nonhuman primates.

Although this case did not classify as such, diagnostic criteria for gastric neuroendocrine carcinoma (gNEC) were reviewed as part of the discussion due to the invasion into the underlying stroma seen on the slide. This feature should have put gNEC on any initial differentials list. Important criteria for gNEC include a single, large, ulcerated mass, usually in the cardia or antrum of the stomach, with poorly differentiated cells arranged in sheets or nests with extensive necrosis.[14] gNEC usually has a spicy mitotic rate (>20 per 1mm^2) and an high Ki67 proliferation index (always >20% and commonly above 70%).[14] The neoplasm in this case was not classified as a gNEC as, although it was invading into the submucosa, it did not have a high mitotic rate, was multifocal, and was not associated with necrosis.

Other gastric and intestinal neuroendocrine neoplasms were reviewed, along with a few important syndromes to keep in mind that are commonly associated with them. For example, gastrinomas that secrete gastrin can do so in such amounts that they stimulate hypersecretion of hydrochloric acid in the stomach, causing gastritis, esophagitis, and/or gastric and duodenal ulceration. This is known as Zollinger-Ellison syndrome. Additionally, carcinoids can be seen in Multiple Endocrine Neoplasia-1 Syndrome. MEN1 results from an autosomal dominant inactivating mutation of the menin gene. Normally, this gene produces menin, a scaffold protein that functions as a critical tumor suppressor, especially in endocrine glands, where it regulates cell growth,

division, DNA repair, and apoptosis.[9] The diagnosis of MEN1 in humans requires either demonstration of the genetic mutation OR least two of the following: parathyroid gland tumor, pituitary tumor, and either gastric, enteric, or pancreatic neuroendocrine tumor (pancreatic are the most common).[12] Alternatively, in humans, MEN1 can also be diagnosed with any one of the listed neoplasms along with demonstration that the affected person also has a first-degree relative with confirmed MEN1. Clinically, primary hyperparathyroidism is the first and most common manifestation of MEN1.[12] Other final points of discussion included the classification of gastric carcinoids (GNETs) into three different types, each of which was kindly covered in the contributor's comment.

References:

1. Albers TM, Alroy J, McDonnell JJ, Moore AS. A Poorly Differentiated Gastric Carcinoid in a Dog. *J Vet Diagn Invest*. 1998;10(1):116-118.
2. Aloisio, F, Dick EJ, Hubbard, GB. Primary hepatic neuroendocrine carcinoma in a baboon (*Papio sp*.). *J Med Primatol*. 2009;38:23-26.
3. Bousquet T, Bravo-Araya M, Davies JL. Gastric neuroendocrine carcinoma (carcinoid) in a ferret (*Mustela putorius furo*). *Can Vet J.* 2022;63(11):1109-1113.
4. Giddens WE, Dillingham LA. Primary Tumors of the Lung in Nonhuman Primates; Literature Review and Report of Peripheral Carcinoid Tumors of the Lung in a Rhesus Monkey. Vet Pathol. 1971;8(5-6):467-478.
5. Hirata A, Miyamoto Y, Kaneko A, Sakai H, Yoshizaki K, Yanai T, Miyabe-Nishiwaki T, Suzuki J. Hepatic neuroendocrine carcinoma in a Japanese macaque (*Macaca fuscata*). *J Med Primatol*. 2019;48(2):137-140.
6. LaDouceur EB, Argue A, Garner MM. Alimentary Tract Neoplasia in Captive Bearded Dragons (*Pogona* spp). *J Comp Pathol*. 2022;194:28-33.
7. Lau DT, Spinelli JS. A spontaneous carcinoid tumor in a cynomolgus monkey, *Macaca fascicularis*. *Lab Anim Care*. 1970;20(6):1145-8.
8. Majka JA, Sher S. Spontaneous gastric carcinoid tumor in an aged Sprague-Dawley rat. *Vet Pathol*. 1989;26(1):88-90.
9. Matkar S, Thiel A, Hua X. Menin: a scaffold protein that controls gene expression and cell signaling. *Trends Biochem Sci*. 2013;38(8):394-402.
10. Oh SW, Chae C, Jang D. Spontaneous gastric carcinoid tumors in the striped field mouse (*Apodemus agrarius*). *J Vet Med Sci*. 1997;59(8):703-6.
11. Ritter JM, Garner MM, Chilton JA, Jacobson ER, Kiupel M. Gastric Neuroendocrine Carcinomas in Bearded Dragons (*Pogona vitticeps*). Veterinary Pathology. 2009;46(6):1109-1116.
12. Singh G, Mulji NJ, Jialal I. Multiple Endocrine Neoplasia Type 1. [Updated 2023 Jul 10]. In: StatPearls [Internet]. Treasure Island (FL): StatPearls Publishing; 2025.
13. Snell KC, Stewart HL. Spontaneous diseases in a closed colony of *Praomys (Mastomys) natalensis*. *Bull World Health Organ*. 1975;52(4-6):645-50.
14. Uccella S, La Rosa S. Neuroendocrine neoplasms of the stomach. Update on diagnostic criteria, classification, and prognostic markers. *Virchows Arch*. Published online November 22, 2025.
15. Uzal FA, Plattner BL, Hostetter JM. Alimentary system. In: Maxie MG, ed. *Jubb, Kennedy and Palmer's Pathology of Domestic Animals.* Vol 2. 6th ed. St. Louis, MO: Elsevier; 2016:105-106.

Wardlaw R, Smith JW. Gastric carcinoid tumors. *Ochsner J*. 2008;8(4):191-6.

CASE III:

Signalment:
Adult female wild mouse (*Mus musculus*)

History:
This wild mouse was found dead in a primate enclosure.

Gross Pathology:
The aorta was lacerated at the level of T8-T9 where the spinal column was severely dislocated and the thoracic cavity contained a large blood clot.

Laboratory Results:
N/A

Microscopic Description:
Few acinar and stromal cells with markedly enlarged nuclei and abundant cytoplasm (cytomegaly) with 8-12 µm eosinophilic intranuclear inclusions were scattered throughout the submandibular salivary gland with accompanying lymphoplasmacytic infiltration in several regions.

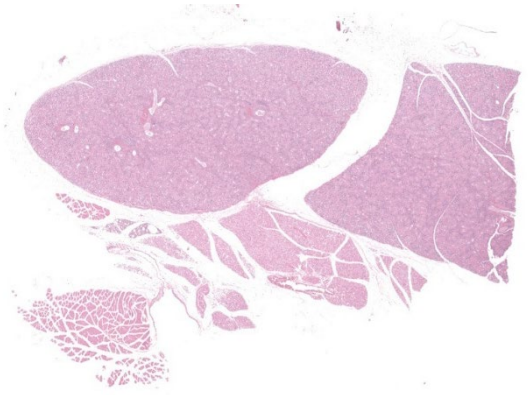

Figure 3-1. Mandibular salivary gland, mouse: One section of the mandibular gland, with associated brown fat and skeletal muscle, is submitted for examination. (HE, 20X)

Contributor's Morphologic Diagnoses:
Sialoadenitis, multifocal, subacute to chronic, mild with epithelial and stromal cytomegaly and intranuclear inclusions (cytomegalovirus)

Contributor's Comment:
Although traumatic laceration of the thoracic aorta with resultant hemothorax was considered the cause of death, infection with mouse cytomegalovirus (MCMV) was a prominent incidental finding in this wild mouse. Wild mice are commonly infected with MCMV, a DNA virus in the family *Herpesviridae*, subfamily *Betaherpesvirinae*, and genus *Muromegalovirus*.[6] Several genetically distinct strains of MCMV exist within wild mouse populations, and mixed infections of single mice are not uncommon. In fact, up to four genetically distinct strains of MCMV have been isolated from a single wild mouse.[3]

The most frequently encountered lesions occur in the submandibular salivary glands and rarely in the parotid glands, with excretion in saliva serving as the primary means of transmission through grooming and biting activities. Typical histological findings include eosinophilic intranuclear and intracytoplasmic inclusions in acinar epithelial cells with cytomegaly and interstitial lymphoplasmacytic inflammation.[6] Intranuclear inclusions result from viral DNA replication within the nuclei of infected cells, while intracytoplasmic inclusions represent replication processes that occur in the cytoplasm, including production of the capsid protein.[8]

As resistance typically evolves after weaning, overt disease and disseminated lesions occur

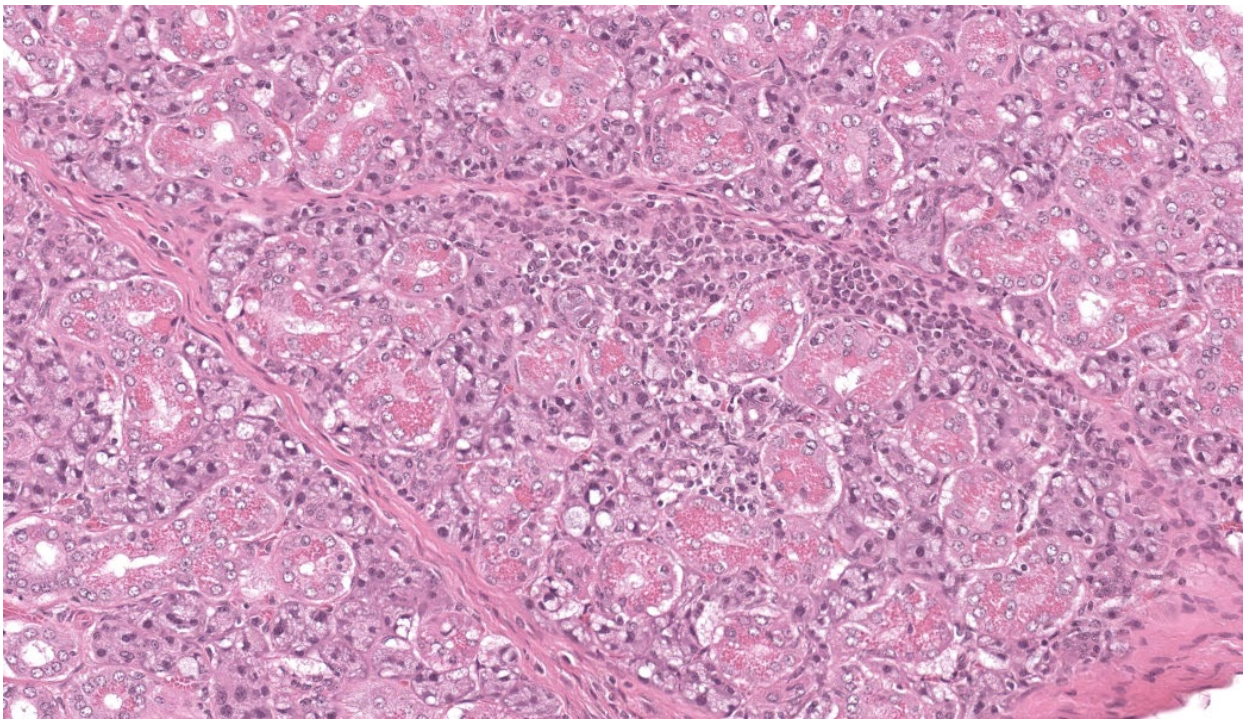

Figure 3-2. Mandibular salivary gland, mouse: The salivary gland interstitium is multifocally infiltrated by moderte numbers of lymphocytes, plasma cells and macrophages. (HE, 365X)

infrequently in naturally infected mice. Neonates are more susceptible to severe disease which may result in encephalitis,
retinitis, pneumonia, hepatitis, myocarditis, adrenalitis and haemopoietic failure. MCMV causes lifelong, persistent infections with intermittent reactivation and viral shedding at times of host immunosuppression. Latent virus in mice may be found in the salivary glands and in other tissues including lung, spleen, liver, kidney, heart, adrenal glands, and myeloid cells.[6]

The betaherpesviruses are highly host specific. Natural infections of cytomegalovirus occur in primates and guinea pigs as well as mice. Rhesus cytomegalovirus (macacine herpesvirus-3) is the most common opportunistic viral infection in rhesus macaques infected with simian immunodeficiency virus.[1] It causes multiorgan dysfunction, with interstitial pneumonia, encephalitis, gastroenteritis and lymphadenitis being most common.[2] In guinea pigs, lesions are largely regarded as incidental findings at necropsy and usually confined to the salivary ductal epithelial cells.[8]

As the course of MCMV infection in mice has similarities to the course of human cytomegalovirus (HCMV) infection, MCMV has been extensively studied and used as a model of the human disease. Credited as the "mother of cytomegalovirus," M. G. Smith first isolated MCMV from the salivary glands of naturally infected laboratory mice in 1954 and propagated it in cell culture.[7] Most laboratory studies have utilized the original Smith strain of MCMV, or derivates thereof, which may not accurately reflect the natural biology of MCMV strains. Nevertheless, the intense scrutiny of MCMV as a model system has shed considerable light on disease pathogenesis.[6]

Investigations into the variable susceptibility of mouse strains to MCMV infection have

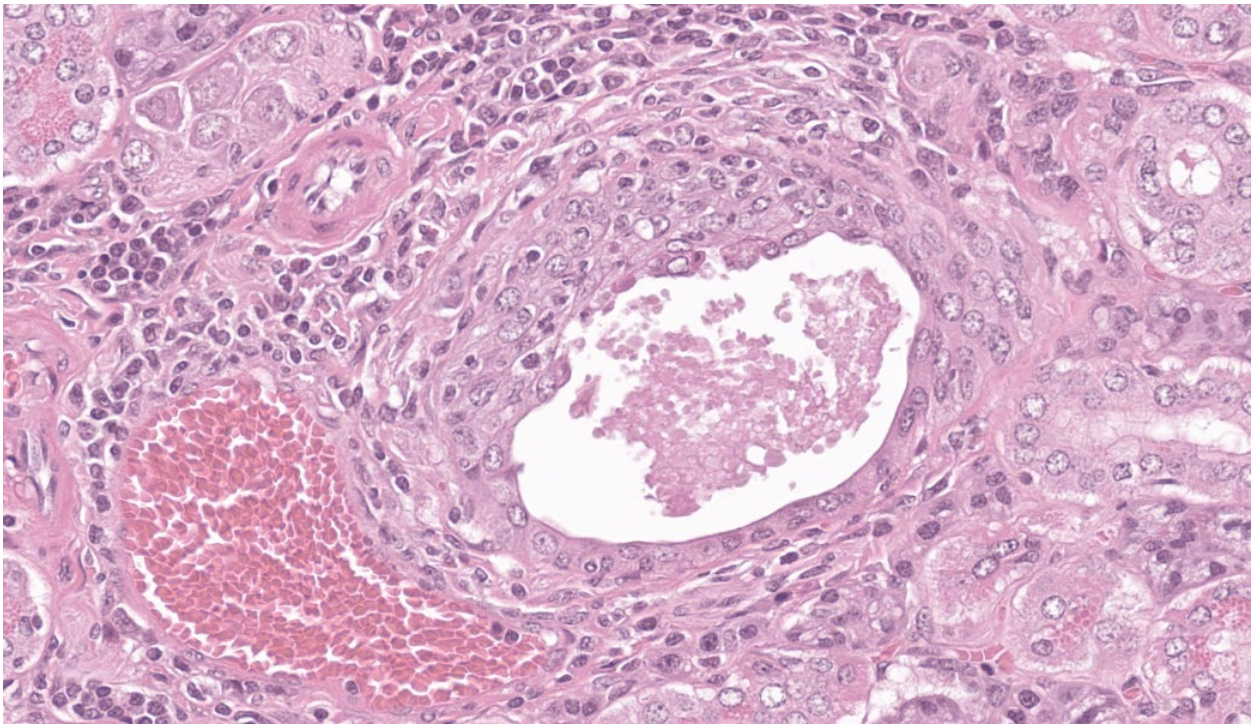

Figure 3-3. Mandibular salivary gland, mouse: There is multifocal necrosis of acinar epithelium with attenuation of remnant epithelium and accumulation of eosinophilic debris within the lumen. (HE, 650X)

shown that innate immune function, in particular the effectiveness of the natural killer (NK) cell response, is the key determinant of resistance to the initial infection and the suppression of viral replication. For example, C57BL/6 (B6) mice are generally considered resistant to MCMV due to the expression of Cmv-1 encoded Ly49H, an NK cell-activating receptor that recognizes the m157 viral protein at the surface of MCMV-infected cells. Activated NK cells suppress the infection by direct lysis of infected cells and by producing cytokines to mediate T-cell responses.[4] Other genetically resistant mouse strains include B10, CBA and C3H mice, while susceptible strains include BALB/c and A strain mice. Susceptibility of wild mice to MCMV strains that circulate in wild populations is attributed to m157 proteins that are unable to activate NK cells via Ly49H.[9] Humoral immunity is relatively unimportant in controlling MCMV infection.

Contributing Institution:
Wake Forest School of Medicine
Department of Pathology, Section on Comparative Medicine
Medical Center Boulevard, Winston-Salem, NC 27157
www.wakehealth.edu

JPC Diagnoses:
Salivary gland: Sialoadenitis, lymphoplasmacytic, chronic, multifocal, mild, with epithelial karyomegaly and intranuclear viral inclusions.

JPC Comment:
This case provided an excellent example of a truly classic lesion that every pathologist should be able to recognize and should come to the forefront of the mind when presented with a slide of murine salivary gland. The contributor provided a great comment on cytomegaloviruses and covered much of what was taught during this case in conference.

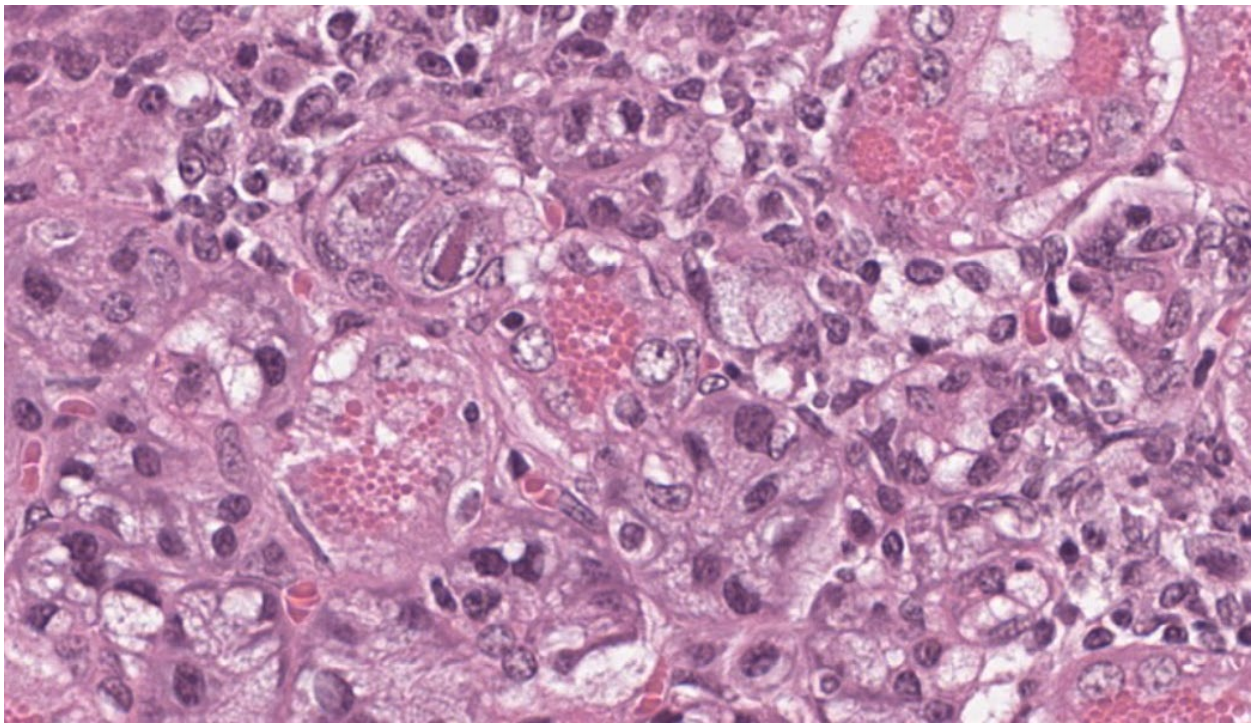

Figure 3-4. Mandibular salivary gland, mouse: Rare acinar cells demonstrate karyomegaly with a single oblong intranuclear cytomegaloviral inclusion which is surrounded by a clear halo. (HE, 1221X)

The submandibular salivary gland in mice (and multiple other species) is a mixed gland with both serous and mucinous glands. In male mice, the submandibular salivary glands are larger than those in female mice and contain brightly eosinophilic, prominent granules in the ductal epithelial cells. Don't forget, though, that those granules can also be seen in pregnant females. B6-strain mice are resistant to infection with CMV, but DBA2 and BALB/C mouse strains are susceptible due to their immune bias towards a Th2 (humoral) response. A subdued Th1 (cell-mediated) immune response results in less effective defense against intracellular pathogens, such as viruses. Th2 cells produce cytokines IL-4 and IL-10, which inhibit the development and function of Th1 cells and their key cytokines, which include interferon-gamma (IFN-γ). A strong IFN-γ response is essential for activating cell-mediated immunity and effectively eliminating virus-infected cells.

While the tissue identification and diagnosis in this case were straightforward, there were some other structures on the slide that served as an excellent reminder of mouse anatomy. Mammary tissue in mice is extensive and can be as far cranial as the submandibular area. Mammary glands are frequently seen in association with the submandibular salivary gland, often hanging out in the subcutaneous tissues. Another primary differential for viral inclusions in the salivary glands of mice is murine polyomavirus (MmusPyV-1). This double-stranded DNA virus is, as the name implies, associated with the development of multiple neoplasms in infected mice. While not all polyomaviruses cause neoplasm development, mouse polyomavirus is well-known to do so. Hamster polyomavirus is similar.

One other important betaherpesvirus of note from discussion is suid herpesvirus-2 (porcine

roseolovirus), which causes necrotizing rhinitis and abortions in swine and can be lethal to humans.[5]

References:

1. Assaf BT, Knight HL, Miller AD. Rhesus cytomegalovirus (Macacine herpesvirus 3)-associated facial neuritis in simian immunodeficiency virus-infected rhesus macaques (*Macaca mulatta*). *Vet Pathol.* 2015;52(1):217-223.
2. Baskin GB. Disseminated cytomegalovirus infection in immunodeficient rhesus monkeys. *Am J Pathol*. 1987;129(2):345-352.
3. Booth M, et al. "Molecular and Biological Characterization of New Strains of Murine Cytomegalovirus Isolated from Wild Mice." *Archives of Virology*. 1993:132(1-2);209–220.
4. Fodil-Cornu N, et al. "Ly49h-Deficient C57BL/6 Mice: A New Mouse Cytomegalovirus-Susceptible Model Remains Resistant to Unrelated Pathogens Controlled by the NK Gene Complex." *Journal of Immunology*. 2008:181(9);6394–6405.
5. Hansen S, Menandro ML, Franzo G, et al. Presence of porcine cytomegalovirus, a porcine roseolovirus, in wild boars in Italy and Germany. *Arch Virol*. 2023;168(2):55.
6. Lathbury LJ, et al. "Effect of Host Genotype in Determining the Relative Roles of Natural Killer Cells and T Cells in Mediating Protection against Murine Cytomegalovirus Infection." *Journal of General Virology*. 1996:77(10);2605–2613.
7. Percy DH, Barthold SW. *Pathology of Laboratory Rodents and Rabbits*. 3rd ed. Ames, IA: Blackwell Publishing; 2007:222.
8. Reddehase, MJ. "Margaret Gladys Smith, Mother of Cytomegalovirus: 60th Anniversary of Cytomegalovirus Isolation." *Medical Microbiology and Immunology*. 2015:204(3);239–241.
9. The Joint Pathology Center, Wednesday Slide Conference 2014-2015, Conference 14, Case: 01." *Askjpc.org*. 2015.
10. Voigt V, et al. "Murine Cytomegalovirus M157 Mutation and Variation Leads to Immune Evasion of Natural Killer Cells." *Proceedings of the National Academy of Sciences of the United States of America*. 2003:100(23);13483–13488.

CASE IV:

Signalment:

5-week-old, female, B6.129S4-C3^{tm1Crr}/J mouse

History:

This female targeting a mutation in the complement component C3 (C3 KO) was 5 weeks old, and she had shown an abnormal enlarged abdomen (homogenous, firm but not very hard to touch). Apart from that she was in normal general condition, with no signs of dehydration nor malnutrition and no signs of diarrhea. Pregnancy is excluded since the animal has been kept in a stock cage with other females.

Gross Pathology:

A fresh carcass was received. No external lesions were observed apart from an enlarged abdomen, which was firm upon palpation.
Abdominal cavity: The abdominal cavity contained a moderate amount of clear, pale-yellow fluid.

Kidney: The left kidney was markedly enlarged, measuring approximately 8x5x4mm, along with an associated diffuse dilation of the left ureter (appr. 5mm in diameter). The left ureter and left kidney were transparent and filled with clear fluid (interpreted as urine). Renal parenchyma was not evident. A hole of approximately 5mm in length was observed in the left renal capsule. Size, surface and color of the right kidney appeared unremarkable, but on cut section, a moderately dilated renal

Figure 4-1. Kidney and ureter, B6.129S4-C^{3tm1Crr}/J mouse: The left kidney is markedly enlarged and transparent, measuring approximately 8 x 5 x 4 mm, as is the left ureter (appr. 5 mm in diameter). These structures are filled with urine. (Photo courtesy of: Institute of Animal Pathology, Vetsuisse Faculty – University of Bern, www.itpa.vetsuisse.unibe.ch)

pelvis was noted. Other observed organs were macroscopically unremarkable.

Laboratory Results:
N/A.

Microscopic Description:
Left kidney: The left kidney is composed of multiple, largely dilated cavities that divide the kidney into numerous islands of parenchyma. These cavities are lined by 2–4 layers of cuboidal to highly columnar, eosinophilic epithelial cells with no mitotic activity (collecting ducts). Few sloughed epithelial cells and erythrocytes are present in the lumen of these ducts. The parenchyma contains islands of immature glomeruli with peripheral nuclei, poorly developed capillaries, and thickened Bowman's capsule (vimentin positive). Primitive tubules are lined by large basophilic cuboidal epithelial cells with minimal or absent lumina. Other areas within the parenchyma consist of mature tubules and glomeruli with some tubules showing mild dilation and intraluminal protein casts. Collecting duct-like structures are multifocally surrounded by loosely arranged mesenchymal tissue (primitive mesenchyme). The interstitium is multifocally expanded by fibrous connective tissue and some areas are infiltrated by low to intermediate numbers of lymphocytes, plasma cells, macrophages, and occasional neutrophils. Some arteries are very prominent (large) with thickened media, and they appear tortuous. A medium sized artery is surrounded and infiltrated by inflammatory cells predominantely macrophages, neutrophils and occasionally multinucleated giant cells within adventitia, media and intima (transmural). Diffuse proliferation of fibroblasts and deposition of fibrin within the vessel wall is observed. Occasionally, the tunica intima is disrupted. Endothelial cell proliferation is evident with clustering of endothelial cells attempting to recanalize the affected lumina.

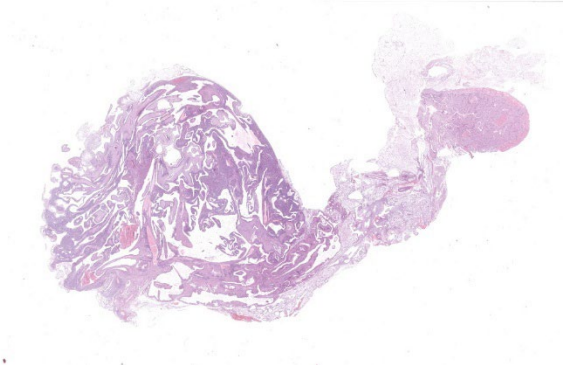

Figure 4-2. Kidney and ureter, B6.129S4-C^{3tm1Crr}/J mouse: One section of the kidney and ureter are submitted for examination. The kidney is a cystic mass (or mess, if you prefer) and has collapsed on itself in the cassette, resulting in the numerous cystic spaces within the parenchyma. A similar change is present in the markedly dilated ureter. (HE, 16X)

Left ureter: Multiple longitudinal and cross-sections of the ureter are present, consisting of urothelium, lamina propria, a smooth muscle layer, and an outer adventitial layer. The peri-ureteral mesenchymal tissue similar to persistent mesenchyme was observed surrounding left ureter and multifocally contains fibrin and exhibits multifocal moderate hemorrhage, and is infiltrated by inflammatory cells, predominantly neutrophils and macrophages, with the presence of hemosiderophages.

Contributor's Morphologic Diagnoses:
Left kidney:

1. Multicystic renal dysplasia with focal rupture of the capsule.
2. Mild to moderate multifocal chronic lymphoplasmacytic tubulointerstitial nephritis.
3. Severe diffuse chronic histiocytic arteritis

Contributor's Comment:
Here, we present an interesting case of unilateral renal dysplasia with unusual cystic dilation of the pelvis and collecting ducts in laboratory mice. Renal dysplasia is well-documented in domestic animals due to its clinical significance; however, the condition has been rarely reported in rodents. Among rodents, renal dysplasia has been reported in a Wistar rat, a Sprague Dawley rat and a Syrian hamster.[5,7,9] To the best of our knowledge, this is the first reported spontaneous occurring case of renal dysplasia in mice.

Renal dysplasia is a congenital or neonatal developmental anomaly of the kidney that results from disruption of the normal development of the collecting duct system.[3] The disease is often congenital, caused by alterations in the renal branching morphogenesis, which occur due to changes in transcription factors, growth factors, and cell surface signaling peptides.[3] It can also be caused by disease in the early neonatal period, before differentiation of the nephrogenic tissue is completed. This is true in species, which have an active subcapsular nephrogenic zone at birth such as cats, dogs, and pigs.[3] In mice, nephrogenesis begins before day 11 of gestation and is completed at birth, whereas in dogs nephrogenesis is completed by post-natal day 14, and even later by post-natal day 21 in pigs and rabbits.[4] This suggests that renal dysplasia in mice is more

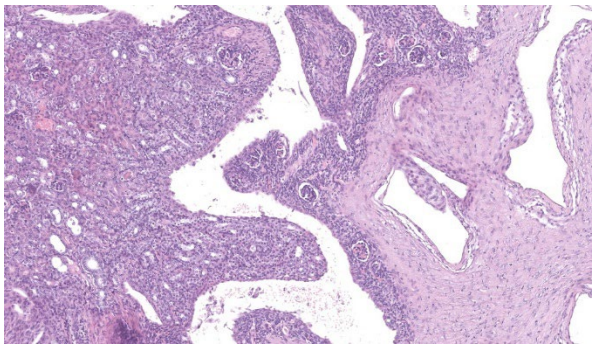

Figure 4-3. Kidney, B6.129S4-C3^{tm1Crr}/J mouse: The cystic nature of the kidney makes identification of normal architecture difficult. The cortex is easily identified due to the presence of glomeruli. As is typical in hydronephrosis, the medulla is markedly fibrotic, and likely represented at left in this distorted kidney. (HE, 163X)

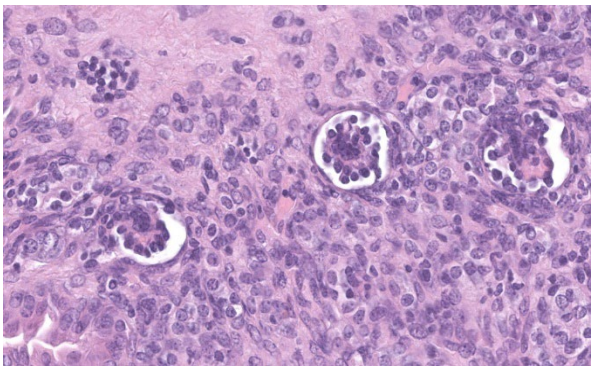

Figure 4-4. Kidney, B6.129S4-C3^{tm1Crr}/J mouse: Within the remnant cortex, numerous small glomeruli with peripheral nuclei (fetal glomeruli) are present.(HE, 663X)

likely to result from congenital anomalies rather than neonatal developmental abnormalities.

Grossly, dysplastic kidneys are usually misshapen, fibrosed with thick-walled cysts and dilated tortuous ureters.[3] One or both kidneys can be affected and the condition can be clinically silent if unilateral, or embryonically lethal when bilateral.[4] Key histological features of renal dysplasia include structures inappropriate to the stage of development or the presence of anomalous structures, in particular undifferentiated mesenchyme, metanephric blastema, immature glomeruli, blind ending collecting tubules, atypical tubular epithelium, metanephric ducts (lined by cuboidal or columnar epithelium), and metaplastic cartilage or bone (rare in domestic animals).[3,8] These alterations could be masked by compensatory, degenerative or inflammatory changes.[3]

This is a case of unilateral renal dysplasia, including immature glomeruli, primitive tubuli and extensively dilated collecting duct-like structures surrounded by primitive mesenchyme. The presence of proteinaceous casts, extensive fibrosis and interstitial nephritis display secondary changes related to impaired renal function. Defective metanephric differentiation results from abnormal interaction between the uretic bud and metanephric blastema leading to renal dysplasia. Complete failure of initiating ureteric bud induction can be diagnosed histologically by the presence of metanephric ducts surrounded by primitive mesenchyme and dysontogenic tissue formation6. As observed in this case, the presence of fetal glomeruli, persistent mesenchyme, and anomalous tubular structures suggests that induction of metanephric blastema was initiated but failed to progress to full differentiation. This is further supported by the immunohistochemistry findings, which demonstrate the persistence of mesenchymal markers (vimentin) in primitive tubules alongside epithelial differentiation (cytokeratin positivity) in more developed structures.[2]

Renal dysplasia may be accompanied by extrarenal abnormalities including segmental ureteral agenesis of the associated dysplastic kidney and imperforate anus.[3] Ureteral anomalies are frequently associated with renal dysplasia due to the close developmental relationship between the kidney and the collecting system. Reported ureteral abnormalities in cases of renal dysplasia include ectopic ureters, ureteral obstruction with hydronephrosis,

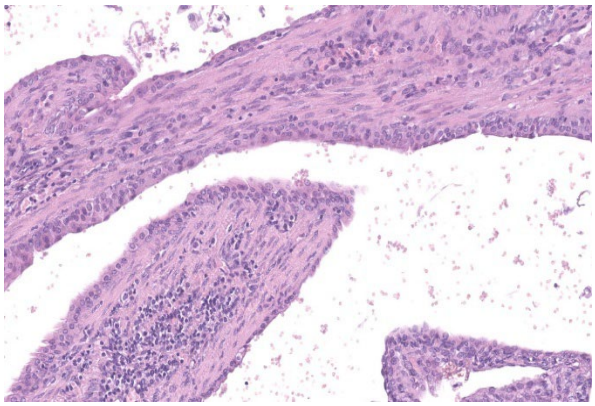

Figure 4-5. Kidney, B6.129S4-C3^{tm1Crr}/J mouse: The cysts are lined with one to multiple layers of urothelium, suggesting a markedly dilated renal pelvis. (HE, 381X)

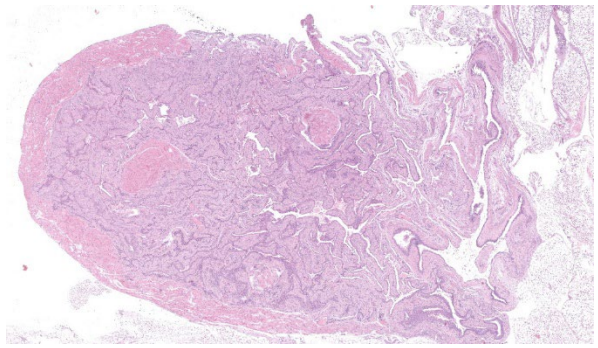

Figure 4-6. Ureter, B6.129S4-C3tm1Crr/J mouse: The collapse of the dilated bladder in the cassette prior to section has resulted in marked complexity in identification (HE, 40X)

hydroureter, and congenital urothelial cell hyperplasia.[10,11] In this case, the ureter associated with the dysplastic kidney is largely dilated and supposably tortuous. While no significant histopathological abnormalities were observed in the ureter itself, its tortuous nature may have impaired urine drainage, potentially leading to progressive renal dilation and rupture.

The observed arteritis in the left kidney is notable. While arteritis is not a common feature of renal dysplasia, it can occur secondary to chronic inflammation or immune-mediated processes such as anti-Glomerular Basement Membrane (GBM) disease.[6] In murine models, polyarteritis nodosa (PAN) is a recognized disease and is characterized by fibrinoid degeneration and necrosis of the tunica media and inflammation of medium and small arteries. This process is mostly associated with neutrophils with or without mononuclear leukocytes and thickening and fibrosis of the vessel wall.[1] Changes often involve arteries of the tongue, head, pancreas, heart, kidneys, mesentery, urinary bladder, uterus, testes, and gastrointestinal tract. Lesions are segmental and their etiology is unknown, but immune complexes have been found in affected vessels.[1] Polyarteritis is an incidental finding which can be associated with segmental infarction of the kidney and scarring.[1]

Although PAN has not yet been described as directly associated with renal dysplasia, chronic kidney injury may predispose to vascular inflammation. In addition, the knockout of C3 in this mouse is associated with defective antibody response to T cell dependent antigens, which might have contributed to disease development. However, arteritis was not observed in other examined organs. Additional investigations into the pathogenesis of arteritis in this case are therefore required.
This is the first case report of spontaneous renal dysplasia in mice. Possible causative relation of dysplastic changes and arteritis observed in this case remains unclear and requires further investigation to elucidate its etiology, particularly in the context of murine models of inflammation, such as C3 knockout.

Contributing Institution:
Institute of Animal Pathology
Vetsuisse Faculty – University of Bern
Länggassstrasse 122
CH-3012 Bern
Switzerland
www.itpa.vetsuisse.unibe.ch

JPC Diagnoses:

1. Kidney: Congenital hydronephrosis, severe, with tubular and glomerular atrophy, interstitial fibrosis, mild lymphoplasmacytic interstitial nephritis.
2. Kidney: Asynchronous maturation, with fetal glomeruli, rare primitive tubules, and primitive mesenchyme.
3. Kidney, arteries and arterioles: Arteritis, neutrophilic and histiocytic, proliferative and necrotizing, chronic, multifocal, severe.

JPC Comment:
This case was fascinating and provided substantial discussion amongst participants, particularly on how best to morph these lesions. The contributor's comment lays out many of the points of debate amongst participants and makes a strong argument for a congenital lesion with prominent secondary changes. The question most attendees were wondering was, "Which parts are congenital and which parts are secondary?"

The large number of fetal glomeruli, presence of few primitive tubules, and occasional primitive mesenchyme, especially in a 5-week old mouse, certainly suggest a degree of renal dysplasia. Mouse kidneys should be completely developed within 4 days of birth (no later than 7 days).[1,5] However, there was debate amongst conference attendees on whether this was a primary renal dysplasia or a secondary delay in maturation due to atrophy caused by congenital hydronephrosis/hydroureter. The fetal glomeruli were strikingly obvious in this case and are characterized by a reduction in the number of capillaries, the presence of podocyte nuclei that palisade around the periphery of a small glomerular tuft, decreased tuft segmentation, and a thick Bowman's capsule. Immature glomeruli are, in a not-so-convoluted kidney, usually best seen in the subcapsular cortex.[1,5] Glomeruli aside, however, while there were rare definitively primitive tubules, most participants thought that many of the tubules were atrophied in response to the severe hydronephrosis rather than truly dysplastic. This was further complicated by the complete lack of medullary distal convoluted tubules. Additionally, there were occasional glomeruli that were mature and the majority of the scant interstitium was relatively developed. As such, many conference participants preferred the term "asynchronous maturation" to describe the spectrum of development seen within the kidney.

Participants wholeheartedly agreed with the contributor regarding the arteritis and similarly diagnosed polyarteritis nodosa (PAN) due to the degree of subintimal proliferation, neutrophilic inflammation, disruption of the elastic laminae, fibrinoid necrosis, and tortuosity of the arteries. Although usually associated with hypertension and most commonly seen in the pancreas, mesentery, and testes, renal PAN is well-documented.[2,4] In this case, it is possible that the degree of hydronephrosis and subsequent pressure atrophy could have contributed to the development of hypertension-like lesions in the arteries, although this is purely speculative and could be a separate process entirely.
The flocculent, cystic spaces made definitive interpretation of this case challenging. The lining of the cystic spaces resembled either persistent metanephric ducts (ducts in the outer medulla lined by pseudostratified, ciliated, columnar epithelium), transitional urothelium, and/or serosa. Metanephric ducts in the medulla potentially represented persistent, incompletely differentiated ureteric bud branches that did not differentiate into normal collecting tubes as they are supposed to, further suggesting a congenital etiology in this condition.[5,10] The presence of serosa-lined spaces implies that some cysts had collapsed in on themselves during processing. Everyone unanimously agreed, however, that this was not polycystic kidney disease.

Differentiating between cystic renal dysplasia and polycystic kidney disease can be challenging, but there are some key differences to be aware of. Cystic renal dysplasia (CRD) is the

most common pediatric renal disease in humans (and is also more common in most animals). It typically has larger cysts that are variably sized and lined by flat-cuboidal epithelium. CRD usually results from urinary tract obstruction and is often unilateral. It occurs sporadically and does not have a defined inheritance pattern like PKD. The characteristic findings for renal dysplasia will be present (fetal glomeruli, primitive tubules, primitive loose mesenchyme, +/- cartilaginous metaplasia, +/- mesenchymal collarettes), and there may or may not be vascular changes.[4,10]

Polycystic kidney disease (PKD), on the other hand, is divided into two subtypes: autosomal dominant PKD (ADPKD) and autosomal recessive PKD (ARPKD). ADPKD is familial, bilateral, and usually does not present until adulthood.[4,10] There is no immature mesenchyme or cartilage present. ARPKD is also familial and bilateral but is generally present at birth.[4] The cysts in ARPKD arise from the collecting ducts and are typically uniform, radially arranged, and fusiform. There is similarly no immature mesenchyme or cartilage.

Due to the differing stages of maturation and the convolution of this case, the JPC consulted with Texas A&M's Dr. Rachel Cianciolo, one of the premier renal experts in veterinary pathology. Her conlusions matched those of some of our more experienced conference particpants in that, while there are abundant fetal glomeruli, there are some that are more mature, but smaller and atrophic. According to Dr. Cianiolo, this supports a diagnosis of a congenital hydronephrosis with delayed renal development, making this case an example of a congenital anomaly of the kidney and urinary tract. She also believes, as did many of our conference attendees, that the cysts are mostly irregular cuts of a severely dilated renal pelvis and calyceal diverticula rather than tubular cysts. Lastly, she stated that, in order to determine if this condition was truly destructive to the kidney and surrounding structures, imaging studies would be necessary. While cost certainly can dictate whether or not imaging will be done in a case, it should be considered in anomalalies like this where imaging could provide additional supportive evidence for a diagnosis, as well as scratch the academic itch to "know"! Many thanks Dr. Cianciolo for sharing her expertise on this interesting case!

References:

1. Baldock RA, Armit C. eHistology image and annotation data from the Kaufman Atlas of Mouse Development. *Gigascience*. 2018;7(2):gix131.
2. Barthold SW, Griffy SM, Percy DH. Pathology of Laboratory Rodents and Rabbits, Fourth Edition. 4th ed. (Barthold SW, Griffey SM, Percy DH, eds.). Wiley; 2016.
3. Carev D, Saraga M, Saraga-Babic M. Expression of intermediate filaments, EGF and TGF-alpha in early human kidney development. *J Mol Histol.* 2008;39(2):227-235.
4. Cianciolo R., Mohr F. Urinary system. In: Maxie M., ed. Jubb, Kennedy, and Palmer's Pathology of Domestic Animals. Vol 2. 6th ed. Elsevier; 2016:376-464.
5. Elmore SA, Kavari SL, Hoenerhoff MJ, et al. Histology atlas of the developing mouse urinary system with emphasis on prenatal days E10.5-E18.5. *Toxicol Pathol*. 2019;47(7):865-886.
6. Frazier KS. Species Differences in Renal Development and Associated Developmental Nephrotoxicity. *Birth Defects Res.* 2017;109(16):1243-1256.

7. Ikeyama Seiichi, Nishibe Tadayuki, Furukawa Satoshi, Goryo Masanobu, Okada Kosuke. Unilateral Renal Dysplasia in a Syrian Hamster. *J Toxicol Pathol.* 2001;14(4):309-312.
8. Jennette JC, Falk RJ, Bacon PA, et al. 2012 revised International Chapel Hill Consensus Conference Nomenclature of Vasculitides. *Arthritis Rheum*. 2013;65(1):1-11.
9. Lee Y-H, Kim D, Park SH, et al. Unilateral non-cystic renal dysplasia in a Sprague Dawley rat. *J Biomed Res*. 2014;15(2):92-95.
10. Picut CA, Lewis RM. Microscopic features of canine renal dysplasia. *Vet Pathol.* 1987;24(2):156-163.
11. Schorsch F, Pohlmeyer-Esch G, Lasserre-Bigot D. Unilateral Renal Agenesis/ Dysplasia associated with Contralateral End-Stage Kidney Disease in Two Wistar Rats. *Eur J Vet Pathol.* 2001;7(3):127-134.
12. The Joint Pathology Center (JPC). JPC Wednesday Slide Conference 2023-2024, Conference 5, Case 04. Published 2023.
13. Yoshida K, Takezawa S, Itoh M, et al. Renal Dysplasia with Hydronephrosis and Congenital Ureteral Stricture in Two Holstein-Friesian Calves. *J Comp Pathol*. 2022;193:20-24.